


## Article

# Subsea Methane Hydrates: Origin and Monitoring of Impact of Global Warming

Vladimir Cheverda<sup>1</sup> , Denis Bratchikov<sup>1</sup>, Kirill Gadylyshin<sup>2</sup>, Elena Golubeva<sup>3</sup>, Valentina Malakhova<sup>3</sup>, Galina Reshetova<sup>3</sup>

<sup>1</sup> Sobolev Institute of Mathematics SB RAS; Novosibirsk av. Acad. Koptug 4, 630090 Russia  
vova\_chev@mail.ru

<sup>2</sup> Trofimuk Institute of Petroleum Geology and Geophysics SB RAS; Novosibirsk av. Acad. Koptug 3, 630090, Russia

<sup>3</sup> Institute of Computational Mathematics and Mathematical Geophysics SB RAS; Novosibirsk av. Acad. Lavrentiev 6, 630090, Russia

\* Correspondence: vova\_chev@mail.ru

**Abstract:** One of the possible mechanisms causing significant emissions of methane into the atmosphere within the Arctic shelf may be the decomposition of gas hydrates. Their accumulations within the Arctic shelf formed during Ice Age almost simultaneously with the formation of permafrost, which contributed to the emergence of a zone of stable existence of gas hydrates. The subsequent flooding of the Arctic shelf led to the degradation of the permafrost and the violation of the conditions for the existence of hydrates. To assess the state of the stability zone, methods of mathematical numerical modeling are used. Standard seismic methods are widely used to localize gas hydrates, but monitoring their physical state requires the development of fundamentally new approaches based on solving multiparameter inverse seismic problems. In particular, the degree of attenuation of seismic energy is one of the objective parameters for assessing the consolidation of gas hydrates: the closer they are to the beginning of decomposition, the higher the attenuation, and hence the lower the quality factor. Thus, the methods of seismic monitoring of the state of gas hydrates in order to predict the possibility of developing dangerous scenarios should be based on solving a multi-parameter inverse seismic problem. This publication is devoted to the presentation of this approach.

**Keywords:** viscoelasticity; seismic attenuation; generalized standard linear solid; multiparameter inverse problem; subsea permafrost; Arctic shelf; methane hydrate stability zone

## 1. Introduction

The Arctic shelf is one of the largest sources of methane emissions into the atmosphere. We believe that one of the possible mechanisms causing this process is the decomposition of methane hydrates preserved in the permafrost zone of continental deposits on the shelf of the Arctic seas during the Ice Age. Indeed, a large amount of methane concentrated in sea bottom sediments in the form of gas hydrates [16,29], which have been formed by the accumulation of dissolved methane under certain P-T conditions for low temperature and high pressure in the methane hydrate stability zone (MHSZ) [29,30]. These conditions exist in marine sediments at water depths of several hundred meters and in the permafrost zone of continental sediments at high latitudes.

Usually in the ocean, gas hydrates appear in bottom sediments at a water depth of more than 500 m, but in the Arctic Ocean, due to low temperatures, gas hydrates can be stable at depths starting from 250 m. Shelf of the Siberian Seas (Kara, Laptev, East Siberian and Chukchi) is an area where the existence of permafrost is possibly due to the suitable PT-conditions. Reliable information on the feasibility of these conditions is obtained from drilling data [25,26]. The presence of permafrost in the bottom sediments provides conditions for the formation of a gas hydrate stability zone at a water depth of less than 100 m [4,18,27,28].

The gas hydrate deposits could be formed during ice ages under subaerial conditions as a result of lowering the ocean level, freezing of exposed bottom sediments and their

subsequent flooding. The reserve of relict gas hydrates of the Arctic shelf is estimated at 65 -1400 PgCH<sub>4</sub> [13,21]. These relict hydrates are especially sensitive to climate change, since the temperature of bottom sediments rises after the shelf is flooded. An increase in temperature or a decrease in pressure due to changes in sea level lead to a violation of the conditions for the stability of methane hydrates, which can lead to the release of large amounts of dissolved and gaseous methane [20,32]. Increased methane emission is also expected as a result of intensified destabilization of gas hydrates and degradation of permafrost on the Arctic shelf in the future [34].

Observational data for 1920-2009 in the shallow part of the shelf and the coastal zone of the Laptev Sea and the East Siberian Sea reflect a significant increase in bottom temperature (up to 2.1 degrees), which began in the mid-1980s [5]. Several events of unprecedented warming in bottom waters thought to be on the verge of freezing all year round have been observed on the central shelf in winter [12,14]. One of the possible explanations for this fact is the degradation of gas hydrates associated with an increase in the temperature of polar waters due to global warming. In turn, the process of melting methane hydrates is inevitably accompanied by their transition from a solid to a gaseous state, which entails an increase in the absorption of seismic energy, especially for transverse waves.

Thus, the temperature dynamics of bottom waters near gas hydrate deposits should be followed very carefully. Its increase can lead to the destabilization of gas hydrate deposits, followed by the rise of a huge amount of gas. In turn, this can provoke the formation of huge gas bubbles with a diameter of several hundred meters, which will threaten both engineering structures and shipping. The localization of such accumulations and the control of their physical condition is a very important task in light of the changing climate of the Arctic, caused by global warming, as well as the expanding activity of geological exploration and the associated increase in the intensity of shipping. and construction of various complex engineering structures like drilling platforms [2]. Therefore, the study of climate change and, as a consequence, possible variations in P-T conditions, together with the localization of gas hydrate accumulations and their monitoring, seems necessary for reliable risk prediction in relation to various sections of the shelf.

In this paper, we will consider the following questions:

- Investigation of the influence of climate warming up to 2200 on the degradation of subsea permafrost and the violation of the conditions for the stable state of methane hydrates in bottom sediments on the example of the East Siberian shelf.
- Estimation of the state of permafrost and MHSZ using a numerical model of heat transfer in shelf bottom sediments and comparison of its results with standard seismic research methods based on the theory of seismic wave propagation in media with attenuation.
- Reconstruction of the state of methane hydrate deposits by multi parameter Full Waveform Inversion (FWI) of seismic data, paying the main attention to reliable reconstruction of attenuation.

We use numerical modeling to assess the state of permafrost and the conditions for the stability of hydrates in bottom sediments. To determine the localization of methane hydrates, standard seismic methods are widely used, but monitoring their physical state requires the development of fundamentally new approaches based on the solution of multi parameter inverse seismic problems.

## 2. Formation of subsea permafrost and methane hydrate stability zones

To carry out the study, we chose an area located within the East Siberian shelf around the New Siberian Islands (see fig.1). Our choice of this area is due to the following factors:

- availability of data on the geological structure, as well as geothermal observations up to a depth of 200 m [9];
- increased methane emissions in this area recorded, both according to shipborne and satellite measurements [35].

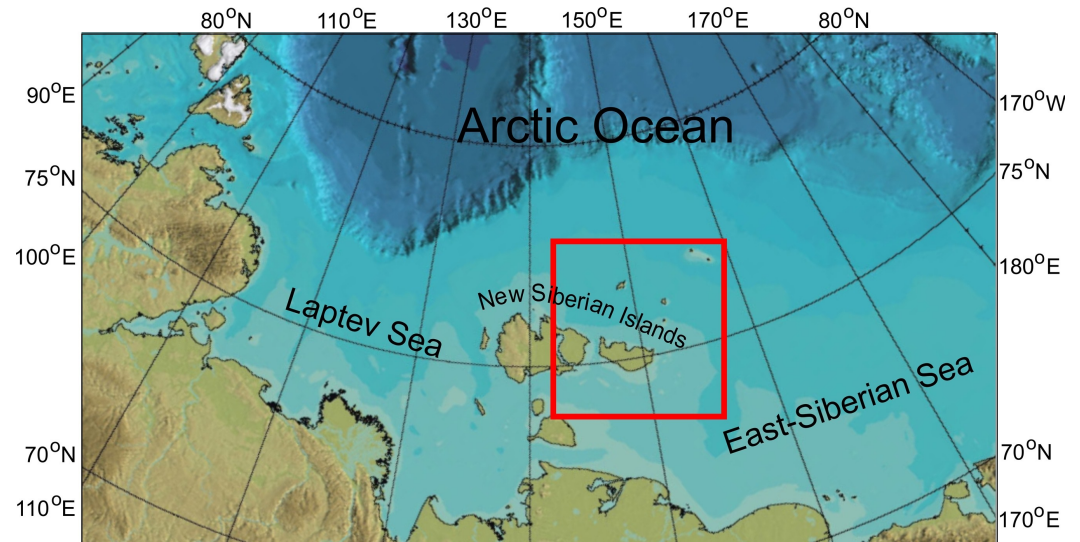


**Figure 1.** Area of gas hydrate study.

To establish the geological structure and thermophysical properties of deposits we used data on the geological structure of the New Siberian Islands [9], fig.1. Their thermophysical characteristics are specified on the base of the lithological composition, geological and genetic affiliation and rocks age according to the data obtained in the adjacent territories [3,7] and consistent with the data obtained in the from the borehole on the land of the New Siberian Islands [9].

### 2.1. Statement of the problem and a brief presentation of the method

To study the processes of formation of subsea permafrost on the Arctic shelf, a one-dimensional model of thermophysical processes in bottom sediments is used, taking into account phase transitions between frozen and thawed deposits [19]. The boundary condition on the surface of bottom sediments is determined by periods of transgressions-regressions, taking into account changes in sea level over the past 200 thousand years [9]. The sea level scenario is based on glacioeustatic curves of World Ocean level fluctuations and their transformation in accordance with regional data [8]. In the eastern sector of the Russian Arctic, there are no paleotemperature data for a number of time intervals. This circumstance does not allow us to construct a scenario for the dynamics of air or rock temperature using only regional data. To this end, it is constructed using the method of using isotopic paleotemperature curves obtained from glacial cores of East Antarctica and Greenland, which reflect the course of global climate fluctuations. The use of isotope paleotemperature curves provides the construction of time-continuous regional curves of air and rock temperature dynamics using discrete regional data [9,19]. The use of isotopic paleotemperature curves provides the construction of time-continuous regional curves of air and rock temperature dynamics using discrete regional data [9,19].

The intensity of the geothermal flux in all numerical simulations was taken equal to  $60 \text{ mW/m}^2$ , which corresponds to the average value of the heat flux for the specific area. To ensure the lower boundary of the computational area does not affect the dynamics of the permafrost, we agreed the maximal depth of the geological model should be 1.5 km. To solve the Stefan problem, the method of catching the front in a node of a spatial grid was used.

Simultaneously with the simulation of the thermal state of bottom sediments, we compute the thermodynamic boundaries of the MHSZ. To determine the equilibrium

pressure ( $P_H$ ) at which methane, water or ice and hydrate can theoretically exist in phase and chemical equilibrium at a given temperature we used the relation [30]:

$$\ln(P_H) = \sum_{n=0...5} a_n(T + T_D)^n$$

where the equilibrium pressure of the hydrate  $P_H$  is in MPa, the temperature  $T$  is in K,  $T_D$  is the shift in the equilibrium temperature which depending on the of salinity [19]. The coefficients  $a_n$  are functions of the ground temperature and are presented in [30].

To implement the model numerically we use the sweep method on a spatial grid with a vertical step of 0.5 m and an implicit time scheme with a step of 1 day. Modeling was carried out for the shelf area of the Laptev Sea with modern depths of 20 m.

## 2.2. Results of numerical simulation

Using the model of heat transfer in bottom sediments with changes in boundary conditions (at the upper boundary), according to the constructed paleogeographical scenario [9], changes in the thickness of the subsea permafrost and MHSZ over the past 200 thousand years (until 1950) were estimated. In numerical calculations for the period 1950 - 2200. the increase in the average annual temperature of bottom water was taken into account, which amounted to 0.02° C per year.

Preliminary modeling of the geocryological situation over a long period (200 thousand years) made it possible to establish the general patterns of its changes. The state of the permafrost depends both on the properties of the deposits that make up the geological section (thermal and physical characteristics, moisture content and salinity), and on the combination of upper and lower boundary conditions and the thermal conductivity of the deposits.

Figure 2 shows temperature profiles in the upper 500 m of bottom sediments at different time horizons up to 2200. According to Figure 2, the maximum differences in the state of permafrost occur after the shelf flooding seven thousand years ago and the transition of continental permafrost to a subaqueous state. At the same time, changes in sediment temperature in the permafrost are insignificant for the last 5 thousand years.

The change in the permafrost thickness over the past 20 thousand years, based on the results of numerical experiments, we present in Fig.3. During the period of the last glacial maximum (about 20 thousand years ago) and the subsequent 5 thousand years, the thickness of frozen deposits reached a maximum of 440 m (Fig.3). The subsequent warming and flooding of the shelf with sea water leads to an increase in the temperature of bottom sediment and thawing of the subsea permafrost (Fig.2). According to model estimates, the thickness of relict permafrost in the bottom sediments of the considered shelf area at a water depth of 20 m was 300 m in modern conditions, Fig. 2, 3. Further warming until 2200 leads to an acceleration of their degradation from the side of the upper boundary, which deepens by 2200 to a depth of 75 m.

The evolution of the methane hydrate stability zone corresponds to the dynamics of P-T conditions, i.e. permafrost dynamics and sea level change. The maximum changes occurred during the warm period seven – six thousand years ago, which was accompanied by sea level rise and flooding of this part of the shelf (Fig.3). The lowering of the MHSZ upper boundary roof showed approximately 60 m (Fig. 3).

According to the results of numerical experiments presented in Fig. 2 the mean annual surface temperature becomes positive (in °C) after 2050. By the end of the 21st century, the boundaries with an average positive temperature of more than 50 m. An increase in the temperature of bottom sediments to accelerate the degradation of permafrost from the upper boundary, Fig. 3. The upper boundary of the subsea permafrost deepens to a depth of 75 m by 2200.

Violation of the conditions for the formation of the MHSZ over the past 6 thousand years, and, consequently, the possible degradation of gas hydrates, leads to the accumulation of methane in the subpermafrost horizons of bottom sediments. The subsequent

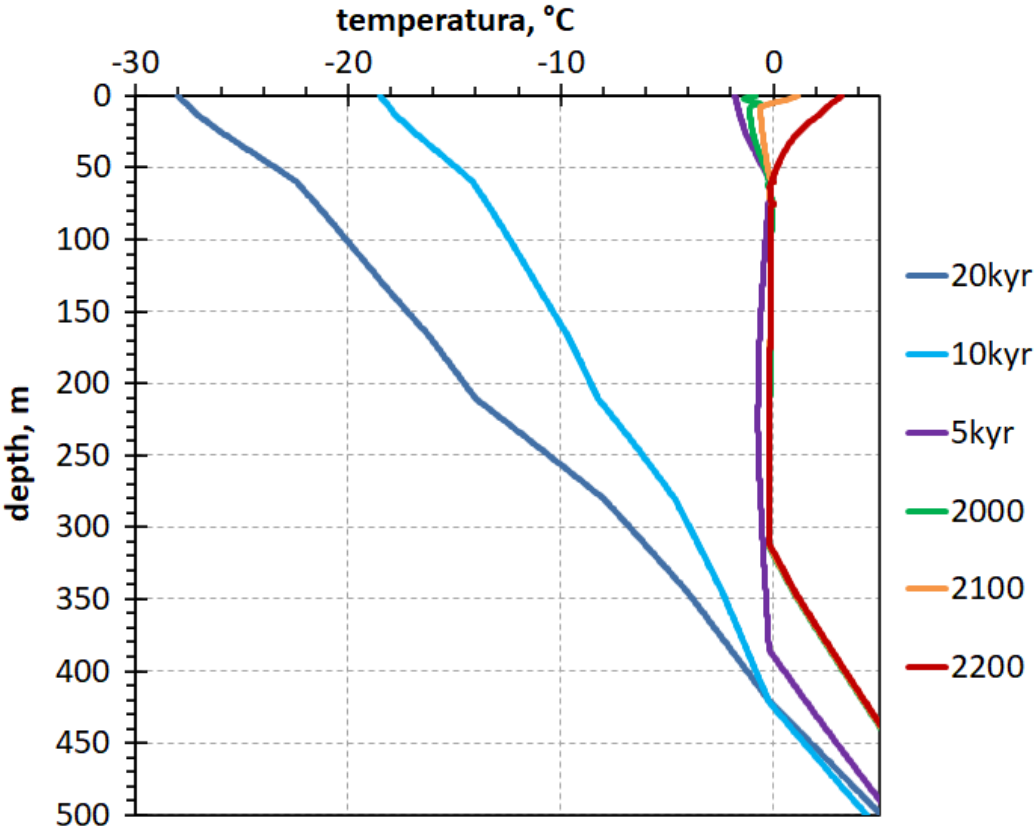


**Figure 2.** Computed vertical temperature profiles in shelf bottom sediments for different time slices: 20 thousand years ago (20kyr), 10 thousand years ago (10kyr), 5 thousand years ago (5kyr) and for 2000, 2100 and 2200, respectively (2000, 2100 , 2200).

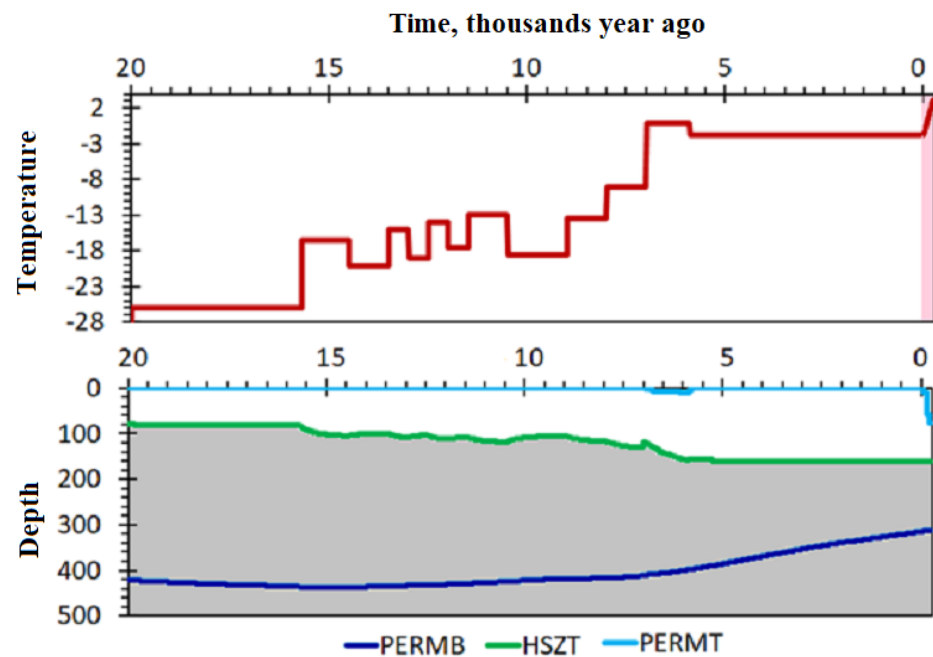


**Figure 3.** Evolution of permafrost and methane hydrate stability zones for the last 20 thousand years based on the results of numerical simulation. The lower boundary of permafrost (PERMB) is the blue line, their upper boundary (PERMT) is the light blue line, the upper boundary of the methane hydrate stability zone (HSZT) is highlighted in green.

destruction of the frozen layer, which occurs in the present period and in the future, may cause an increase in the permeability of bottom sediment and the flow of methane into the atmosphere from areas of the shallow shelf.

### 3. Seismic absorption

In a frozen state, gas hydrates practically do not differ from a pure elastic medium. However, as the temperature rises, they gradually change to a liquid and then to a gaseous state. Naturally, this also changes a number of their physical properties, including the ability to absorb seismic energy. In other words, deposits of gas hydrates from an ideally elastic state pass into a viscoelastic state and then into a liquid and gaseous state. Therefore, it seems quite reasonable to monitor the state of gas hydrate deposits by assessing their absorption properties. Therefore, the mathematical formulation of the problem of detecting gas hydrates and monitoring their state should use the theory of seismic wave propagation in ([31], [23]). It is the absorption variability that will provide us with information about the state of the gas hydrate deposit. Thus, we come to the need to consider a multi-parameter inverse problem of seismic wave propagation, since we need to restore two families of unknown parameters:

- P- and S-wave propagation velocities;
- P- and S-quality factors.

Let us dwell briefly on the representation of the mathematical model of seismic wave propagation in viscoelastic media.



### 3.1. Mathematical model of a viscoelastic medium

The attenuation of seismic energy is characterized by a quality factor determined by the relationship:

$$Q^{-1} = \frac{1}{2\pi} \frac{\Delta E}{E},$$

where  $E$  is the seismic energy per unit volume per unit time, and  $\Delta E$  specifies its loss per unit volume per unit time. As a result of numerous field experiments, a remarkable fact has been established [17]:

the quality factor does not depend on frequency in the seismic frequency range for most geological media.

At present, to describe wave processes in viscoelastic media, the Generalized Linear Solid (GSL) Model is the most widely used, which makes it possible to provide almost any value of the quality factor in a given frequency range (see e.g. [11], Chapter 5 of the book [6]). To do this, several attenuation mechanisms are used and determined by relaxation times for strains and stresses. In this paper, we use this model in the implementation of the  $\tau$  method [1].

The undoubted advantage of the GSL model lies in the possibility of introducing the quality factor independently for S- and P-waves:

- for S-shear waves

$$\mu(\omega) = \mu_r \left( 1 + \frac{i\omega^2 \tau^S}{L} \sum_{l=1}^L \frac{\tau_l}{1 + i\omega \tau_l} \right) = \mu_r (1 + \tau^S S(\omega)) \quad (1)$$

- for P-waves

$$\begin{aligned} \lambda(\omega) + 2\mu(\omega) &= (\lambda_r + 2\mu_r) \left( 1 + \frac{i\omega^2 \tau^P}{L} \sum_{l=1}^L \frac{\tau_l}{1 + i\omega \tau_l} \right) = \\ &= (\lambda_r + 2\mu_r) (1 + \tau^P S(\omega)) \end{aligned} \quad (2)$$

The symbol  $r$  here means that the given value corresponds to frequency.

Formulas (1)-(3.1) lead to the following representations of P- and S-quality factors when one uses  $L$  attenuation mechanisms:

$$Q_{P,S} = \frac{\sum_{l=1}^L \left( 1 + \tau^{P,S} \frac{\omega^2 \tau_l}{1 + \omega^2 \tau_l^2} \right)}{\omega \tau^{P,S} \sum_{l=1}^L \frac{\tau_l}{1 + \omega^2 \tau_l^2}} \quad (3)$$

The  $\tau_l$  parameters determine the relaxation times for stresses in the GSL model used, and have the dimensions of time. The values  $\tau^{P,S}$  determine the values of the quality factor  $Q$  for P- and S-waves.

Thus, the construction of a mathematical model of a viscoelastic medium for a given distribution of quality factors  $Q_{P,S}$  is carried out in two steps:

1. Calculation of the relaxation times  $\tau_l$ , ensuring the constancy of the quality factor by minimizing the functional:

$$\tau_l = \operatorname{argmin} \| \text{const} - Q_{P,S}(\omega) \|$$

2. Determination of the spatial distribution of the relaxation times  $\tau^P$  and  $\tau^S$ , providing the given values of the quality factor  $Q_{P,S}$  in the computational domain.

Let us now consider the wave process caused by a point source within a viscoelastic medium. In terms of temporal frequencies we arrive at the following system of equations:

$$\left\{ \begin{array}{l} \omega^2 \rho u_x + \frac{\partial}{\partial x} \left( ((\lambda + 2\mu)(1 + S\tau^P) \operatorname{div} \vec{u} - 2\mu(1 + S\tau^S) \frac{\partial u_z}{\partial z}) \right) + \\ + \frac{\partial}{\partial z} \left( \mu(1 + S\tau^S) \left( \frac{\partial u_x}{\partial z} + \frac{\partial u_z}{\partial x} \right) \right) = F_1(\omega) G_x(\vec{x} - \vec{x}_0); \\ \frac{\partial}{\partial z} \left( ((\lambda + 2\mu)(1 + S\tau^P) \operatorname{div} u - 2\mu(1 + S\tau^S) \frac{\partial u_z}{\partial z}) \right) + \\ \omega^2 \rho u_z + \frac{\partial}{\partial x} \left( \mu(1 + S\tau^S) \left( \frac{\partial u_x}{\partial z} + \frac{\partial u_z}{\partial x} \right) \right) = \\ = F_2(\omega) G_z(\vec{x} - \vec{x}_0) \end{array} \right. \quad (4)$$

To close the obtained system of equations, it is necessary to introduce a boundary condition on the free surface  $z = 0$ , setting the vertical component of the stress tensor equal to zero there, and also requiring the displacement vector to tend to zero at infinity.

### 3.2. Numerical experiments on modeling seismic waves in viscoelastic media

In order to evaluate how the Q factor variability affects the seismic wave fields, we performed a series of numerical experiments, changing the Q factor in the target group of layers. To do this, we used an elastic model that describes the behavior of the velocities and Q-factors of longitudinal and transverse waves, obtained as a result of research in the area marked with a red square in Fig.1 (see a detailed description in the works [9,10,25]).

The distribution of P-wave velocities used in the simulation can be seen in Fig.4. Unfortunately, we do not have data on the distribution of S-wave velocities on the same vertical profile, so we adopted a fairly common practice, when it is assuming to be equal to the speed of P-waves divided by  $\sqrt{3}$ .

Drilling data proved that the layer at a depth of 200 m contains gas hydrate deposits. In the initial frozen state, gas hydrates are indistinguishable in their mechanical parameters from an ideally elastic medium, however, as the temperature rises, they become less and less consolidated until they are completely decomposed into gas and water. Naturally, in this case, the mechanical properties of the rock also change significantly. Suffice it to say that in terms of its elastic properties, the conglomerate formed during the melting of gas hydrates becomes closer to a mixture of gas and liquid. In particular, this means that transverse waves must be significantly weakened in it, that is, the quality factor  $Q_s$  will tend to zero. It is this property of melting gas hydrates that seems promising to us as a prognostic sign of an approaching catastrophic methane release.

In order to evaluate how much Q-factor reduction affects seismic wave fields, we performed a series of numerical experiments simulating a seismic wave field caused by a point source. In each experiment, we changed the quality factor in the layer at a depth of 200 m (see fig.4), since it was in this layer that gas hydrates were found during drilling. For simulation, we used the previously developed finite difference algorithm based on the  $\tau$ -method, staggered grids and the software created on its basis (see [33] for more detail).

We used a Ricker pulse with a dominant frequency of 25 Hz as a probing signal in a source located on the free surface. In total, three experiments with different quality factors within the target layer at a depth of 200 m. Figure 5 presents the vertical components of the wave field at a distance of 500 m from the source at a point located in the middle of the target layer. Let us note that the first arrivals presented here correspond to a P-wave, which has a predominantly horizontal polarization inside the target layer.



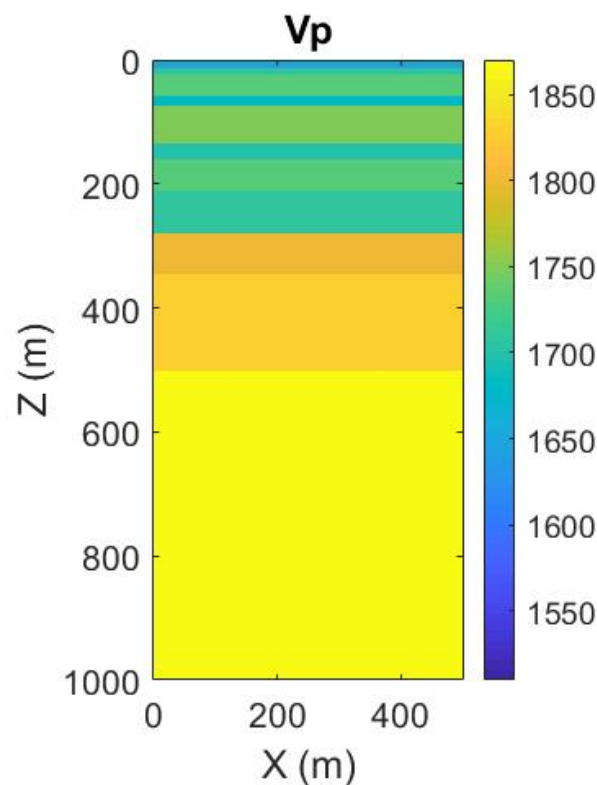


**Figure 4.** P-wave velocities along one of the vertical wells in the study area.

- Seismic trace for elastic medium with no attenuation - this case corresponds to the black line. As one can be sure, The first arrival times exactly fit to those predicted by ray theory for both P- and S-waves.
- The red line corresponds to the same elastic model and the same geometry of the relative position of the source and receiver, but in the target layer the quality factor is 20. As one can see, there are three main differences from the case of a ideal elastic medium:
  1. Increase in phase speed;
  2. Amplitude reduction;
  3. "Spreading" of the signal, which indicates a decrease in the dominant frequency.
  4. The blue curve sets the seismic trace for a Q factor of 10. As you can see, the three differences noted above are only getting stronger.

For each of the obtained synthetic wave fields, we also estimated their global variability as the quality factor changes. It turned out that the relative change of these wave fields reaches 10-13%.

Thus, based on the numerical experiments performed, we can conclude that the variability of the quality factor even in such a narrow layer introduces very significant changes in the seismic wave fields. This allows us to hope for a reliable Q-factor reconstruction and, consequently, for the effective implementation of seismic monitoring of the process of thawing of gas hydrates.

#### 4. Full Waveform Inversion for Viscoelastic Media

Let us now consider the solution of a multiparameter inverse problem for a viscoelastic medium. Let us assume that for a given acquisition we know the solution of the system of equations (4) for the frequency range  $(\omega_1, \omega_2)$ . We will treat this wave field solution as the result of the action of the nonlinear operator  $B$  on the parameters of the viscoelastic medium: the Lamé coefficients  $\lambda, \mu$  and the relaxation times  $\tau^P, \tau^S$ . Thus, the multi-

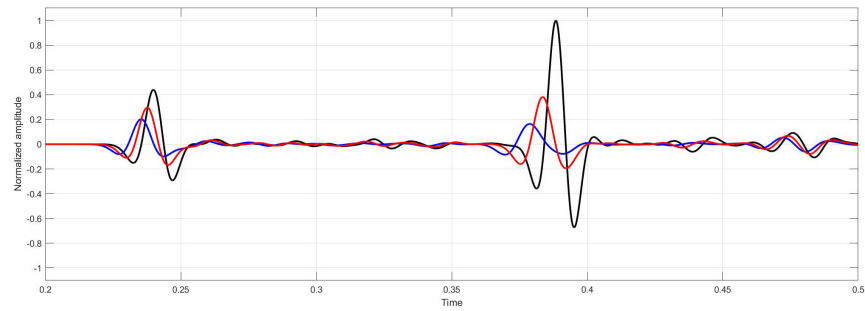


**Figure 5.** Comparison of three seismic traces on the  $z = 0$  line. Black corresponds to a perfectly elastic medium, red corresponds to a target layer with a Q factor of 20, and blue corresponds to a target layer with a Q factor of 10.

parameter inverse problem for viscoelastic media is nothing but the inversion of the nonlinear operator  $B$  implicitly introduced by (4):

$$\vec{u}(x_r, z_r; x_s, z_s; \omega) = B[\lambda, \mu, \tau^P, \tau^S], \quad \omega_1 \leq \omega \leq \omega_2 \quad (5)$$

Let us search for the solution of this equation (5) by nonlinear least squares minimizing the objective functional, characterizing the discrepancy between measured and synthetic data:

$$\Phi[\lambda, \mu, \tau^P, \tau^S] = \|\vec{u}(x_r, z_r; x_s, z_s; \omega) - B[\lambda, \mu, \tau^P, \tau^S]\|^2 \quad (6)$$

To solve such a problem, the people usually use some local minimization techniques reducing to computations of the gradient (5). In particular, it is worth mentioning the conjugate gradient method and its various modifications, (see [15,24]), or quasi-Newtonian methods (see Chapter 6 in the book [22]).

The kernel of gradient-type methods is construction of an iterative process that minimizes the objective functional (6) and updating the resulting solution. One of the simplest and most popular approaches for this are the steepest descent, conjugate gradient and quasi-Newton methods. The key idea here is the search of the next approximation along some direction, whose construction is based on the knowledge of the current gradient. The simplest technique here is the steepest descent in which the next value of the parameters is sought along the direction of the antigradient providing the fastest decrease in the objective functional:

$$[\lambda_{k+1}, \mu_{k+1}, \tau_{k+1}^P, \tau_{k+1}^S] = [\lambda_k, \mu_k, \tau_k^P, \tau_k^S] - \alpha_k \nabla \Phi[\lambda_k, \mu_k, \tau_k^P, \tau_k^S]. \quad (7)$$

The step length  $\alpha_k$  is found as a result of one-dimensional minimization:

$$\alpha_k = \arg \min \Phi \left[ [\lambda_k, \mu_k, \tau_k^P, \tau_k^S] - \alpha \nabla \Phi \right]. \quad (8)$$

However, as we have already mentioned, the steepest descent method has a number of disadvantages that significantly slow down and sometimes stop its convergence for high-dimensional problems and complex functionals. That is why various modifications are often used instead of it, such as various implementations of the conjugate gradient method, quasi-Newtonian methods and others. In this paper, we are looking for a minimum point using the conjugate gradient method.

Let us now describe numerical experiments on the application of full wave form inversion in a viscoelastic medium. To do this, we will use the model presented in figure 4. Let's start by getting the ratios for calculating the gradient.

#### 4.1. Gradient of the objective functional in the problem of Full Waveform Inversion in viscoelastic media

Let's start with the derivation of relations that determine the gradient of the objective functional  $\Phi$  in accordance with the representation (6). As a rule, the standard deviation of the discrepancy between the acquired and the synthetic data simulated for the current model is used, so the objective functional can be represented as  $L_2$  dot product:

$$\Phi[\lambda, \mu, \tau^P, \tau^S] = \left( \vec{u}(x_r, z_r; x_s, z_s; \omega) - B[\lambda, \mu, \tau^P, \tau^S], \vec{u}(x_r, z_r, \omega) - B[\lambda, \mu, \tau^P, \tau^S] \right) \quad (9)$$

By definition, the gradient defines the linear part of the increment of the objective functional, that is:

$$\begin{aligned} \Phi[\lambda + \delta\lambda, \mu + \delta\mu, \tau^P + \delta\tau^P, \tau^S + \delta\tau^S] &= \Phi[\lambda, \mu, \tau^P, \tau^S] + \nabla\Phi[\lambda, \mu, \tau^P, \tau^S] \\ &(\delta\lambda, \delta\mu, \delta\tau^P, \delta\tau^S) + O(\delta\lambda^2, \delta\mu^2, (\delta\tau^P)^2, (\delta\tau^S)^2) = \Phi[\lambda, \mu, \tau^P, \tau^S] + \\ &+ 2\Re \left\{ \vec{u}(x_r, z_r; x_s, z_s; \omega) - B[\lambda, \mu, \tau^P, \tau^S], \frac{\partial B}{\partial \lambda} \delta\lambda + \frac{\partial B}{\partial \mu} \delta\mu + \frac{\partial B}{\partial \tau^P} \delta\tau^P + \frac{\partial B}{\partial \tau^S} \delta\tau^S \right\} \end{aligned} \quad (10)$$

Thus, we obtain the following expression for representing the linear part of the increment of the objective functional, that is, for its gradient:

$$\begin{aligned} \nabla\Phi < \delta\lambda, \delta\mu, \delta\tau^P, \delta\tau^S > &= \left( \left( \frac{\partial B}{\partial \lambda} \right)^* < \vec{u} - B >, \delta\lambda \right) + \\ &\left( \left( \frac{\partial B}{\partial \mu} \right)^* < \vec{u} - B >, \delta\mu \right) + \left( \left( \frac{\partial B}{\partial \tau^P} \right)^* < \vec{u} - B >, \delta\tau^P \right) + \\ &+ \left( \left( \frac{\partial B}{\partial \tau^S} \right)^* < \vec{u} - B >, \delta\tau^S \right) \end{aligned} \quad (11)$$

Here  $A^*$  denotes the adjoint to the operator  $A$ .

The obtained representation of the objective functional gradient allows us to write down the iteration process that implements the steepest descent method as follows:

$$\lambda_{k+1} = \lambda_k - \alpha_k^\lambda \left( \frac{\partial B}{\partial \lambda} \right)^* \langle \vec{u} - B \rangle \quad (12)$$

$$\mu_{k+1} = \mu_k - \alpha_k^\mu \left( \frac{\partial B}{\partial \mu} \right)^* \langle \vec{u} - B \rangle \quad (13)$$

$$\tau_{k+1}^P = \tau_k^P - \alpha_k^P \left( \frac{\partial B}{\partial \tau^P} \right)^* \langle \vec{u} - B \rangle \quad (14)$$

$$\tau_{k+1}^S = \tau_k^S - \alpha_k^S \left( \frac{\partial B}{\partial \tau^S} \right)^* \langle \vec{u} - B \rangle \quad (15)$$

#### 4.2. Fréchet derivative of the operator $B$

We now give a representation for the formal Frechet derivatives of the operator  $B[\lambda, \mu, \tau^P, \tau^S]$  with respect to the parameters of the viscoelastic medium. We restrict ourselves to constructing a derivative only for the Lamé parameter  $\lambda$ , all other derivatives are constructed according to the same scheme. In order to avoid cumbersome calculations, we write down the system of equations (4) in general form:

$$L(\lambda, \mu, \tau^P, \tau^S) \vec{u}(x, z; x_s, z_s; \omega) = \vec{F}(x, z; x_s, z_s; \omega) \quad (16)$$

Let us now introduce the increment of the parameter  $\lambda$  and the corresponding increment of the wave field  $\delta \vec{u}$ , then, up to the small of the second order, we obtain the following relation connecting these increments:

$$L(\lambda, \mu, \tau^P, \tau^S) \delta \vec{u}(x, z; x_s, z_s; \omega) = -\frac{\partial L}{\partial \lambda} \delta \lambda \vec{u}(x, z; x_s, z_s; \omega) \quad (17)$$

Here  $(x_s, z_s)$  are coordinates of the point source. Let us consider now Green's matrix  $G(x, z; x_s, z_s; \omega)$ , which describes at the point  $(x, z)$  a wave field from the source point of the oriented force at the point  $(x_s, z_s)$ . Let rewrite equation (17) as:

$$\left\{ \begin{array}{l} \omega^2 \rho \delta u_x + \frac{\partial}{\partial x} \left( ((\lambda + 2\mu)(1 + S\tau^P) \operatorname{div} \delta \vec{u} - 2\mu(1 + S\tau^S) \frac{\partial \delta u_z}{\partial z}) \right) + \\ + \frac{\partial}{\partial z} \left( \mu(1 + S\tau^S) \left( \frac{\partial \delta u_x}{\partial z} + \frac{\partial \delta u_z}{\partial x} \right) \right) = -\frac{\partial}{\partial x} \left( \delta \lambda (1 + S\tau^P) \operatorname{div} \vec{u} \right); \\ \frac{\partial}{\partial z} \left( ((\lambda + 2\mu)(1 + S\tau^P) \operatorname{div} \delta \vec{u} - 2\mu(1 + S\tau^S) \frac{\partial \delta u_z}{\partial z}) \right) + \\ \omega^2 \rho \delta u_z + \frac{\partial}{\partial x} \left( \mu(1 + S\tau^S) \left( \frac{\partial \delta u_x}{\partial z} + \frac{\partial \delta u_z}{\partial x} \right) \right) = \\ = -\frac{\partial}{\partial z} \left( \delta \lambda (1 + S\tau^P) \operatorname{div} \vec{u} \right). \end{array} \right. \quad (18)$$

and write down the solution of the resulting system in the form:

$$\delta \vec{u}(x_r, z_r, x_s, z_s; \omega) = \int_D G(x_r, z_r; \xi, \zeta; \omega) \left[ \begin{array}{l} \frac{\partial}{\partial x} [\delta \lambda (1 + S\tau^P) \operatorname{div} \vec{u}] \\ \frac{\partial}{\partial z} [\delta \lambda (1 + S\tau^P) \operatorname{div} \vec{u}] \end{array} \right] d\xi d\zeta \quad (19)$$

Let us suppose the function  $\delta \lambda$  is smooth and vanishes at the boundary of D:

$$\delta \vec{u}(x_r, z_r, x_s, z_s; \omega) = - \int_D \left[ \begin{array}{l} \frac{\partial G(x_r, z_r; \xi, \zeta; \omega)}{\partial x} \\ \frac{\partial G(x_r, z_r; \xi, \zeta; \omega)}{\partial z} \end{array} \right] \delta \lambda (1 + S\tau^P) \operatorname{div} \vec{u} d\xi d\zeta \quad (20)$$

Following the definition of a derivative we conclude, that the solution of the system of equations (18) defines the Fréchet derivative with respect to the parameter  $\lambda$ . All other derivatives with respect to the parameters of the viscoelastic medium are constructed in exactly the same way. To construct adjoint operators, we do the scalar product of both parts of (20) by an arbitrary function  $\phi(x_r, z_r, x_s, z_s, \omega)$ , followed by rearrangement of the integral to extract the scalar product by the function  $\delta \lambda(\xi, \eta)$ .

#### 4.3. Numerical experiments

For numerical experiments, we use the same vertically inhomogeneous model as before (see fig.4), but introduced an additional layer with P- and S-waves attenuation  $q_p$  and  $q_s$  at the depth of 200 meters (see fig.6). When performing numerical experiments for a viscoelastic medium, we set the main task to study the coupling of parameters, therefore, we allowed for variability of both velocities and quality factors. By the connection of parameters, we mean the possibility of their false variability. Let's explain what is meant. Suppose there is a model of a viscoelastic medium with four parameters: P- and S-velocities  $V_p$  and  $V_s$ , and P- and S-absorption  $q_p$  and  $q_s$ . Further, we will assume that we know the initial approximation, which coincides with the true distribution of

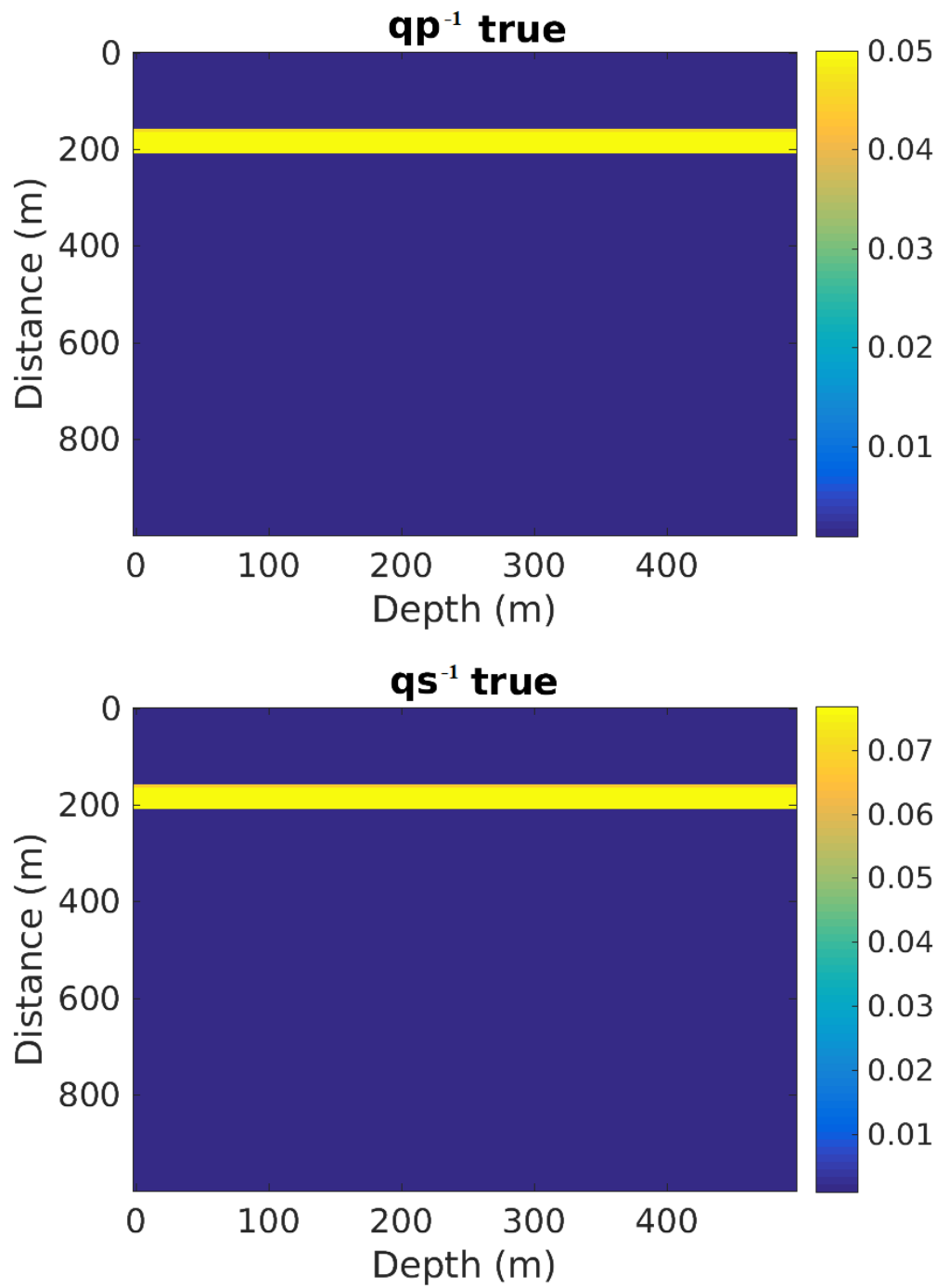


**Figure 6.** Q-factor distribution for P- (top) and S-(bottom) waves

parameters in the medium, except for one of them, for example,  $q_p$ . Then the presence of the coupled parameters means that in the process of solving the inverse problem, we will get a perturbation not only for  $q_p$ , but also for other parameters. Naturally, the coupling of parameters is not allowed when monitoring the state of gas hydrates, since here it is necessary to be sure that the results obtained are true and the obtained change in quality factor is really associated with a change in the physical properties of the geological object under study. As can be seen from the presented results of implementation the FWI in a viscoelastic medium, our approach is free from the mentioned drawbacks.

First of all, let us analyze the results of Q-factor restoration for P- and S-waves, shown in the two upper panels Fig. 7. We note the confident coincidence of the true and reconstructed quality factors, both in terms of their spatial localization and absolute values, as well as the absence of manifestations of their influence on the reconstructed velocities of longitudinal and transverse waves. This allows us to assert that these two groups of parameters are not related when solving the inverse problem by the FWI method.

When performing numerical experiments for a viscoelastic medium, we set the main task to study the coupling of parameters, therefore, we allowed for variability of both velocities and quality factors. By the connection of parameters, we mean the possibility of their false variability. Let's explain what is meant. Suppose there is a model of a viscoelastic medium with four parameters: P- and S-velocities  $V_p$  and  $V_s$ , and P- and S-absorption  $q_p$  and  $q_s$ . Further, we will assume that we know the initial approximation, which coincides with the true distribution of parameters in the medium, except for one of them, for example,  $q_p$ . Then the presence of the coupled parameters means that in the process of solving the inverse problem, we will get a perturbation not only for  $q_p$ , but also for other parameters. Naturally, the coupling of parameters is not allowed when monitoring the state of gas hydrates, since here it is necessary to be sure that the results obtained are true and the obtained change in quality factor is really associated with a change in the physical properties of the geological object under study. As can be seen from the presented results of implementation the FWI in a viscoelastic medium, our approach is free from the mentioned drawbacks.

To conclude this section, we note the monotonic decrease in the objective functional when minimizing by the conjugate gradient method (see Fig.8). This ensures that the iterations will be not stopped before the minimum is reached. .

## 5. Discussion

Global climate warming and anthropogenic impact associated with the intensive industrial development of the Arctic shelf lead to a change in the thermobaric conditions of its bottom layers. As can be seen from the actual data presented in the Introduction and the first chapter, in recent years there has been a steady increase in the temperature of bottom waters with a gradient of 0.02 degrees Celsius per year. In turn, such an increase in temperature leads to a change in thermobaric conditions and immersion to a greater depth of the upper boundary of the gas hydrate stability zone. One of the undesirable consequences of this may be the thawing of permafrost, which retains gas hydrates in a solid state, and their subsequent degradation, accompanied by the release of significant volumes of methane. Therefore, monitoring of methane hydrate deposits in order to control their condition and assess the degree of their thawing is one of the most important tasks to ensure the safe development of the shelf of the Arctic seas.

Methane hydrates located in the stability zone are close in their physical properties to ideally elastic bodies in which there is no absorption of seismic energy. However, with an increase in temperature, thawing begins, leading to a decrease in their consolidation and, consequently, to losses of seismic energy during the propagation of elastic waves. Naturally, the closer the methane hydrates to decomposition, the higher the absorption, and the energy losses for S-waves are much higher than for P-ones.

The most universal and reliable method for solving inverse seismic problems is the Full Waveform Inversion (FWI). The results presented in the article confirm that its application



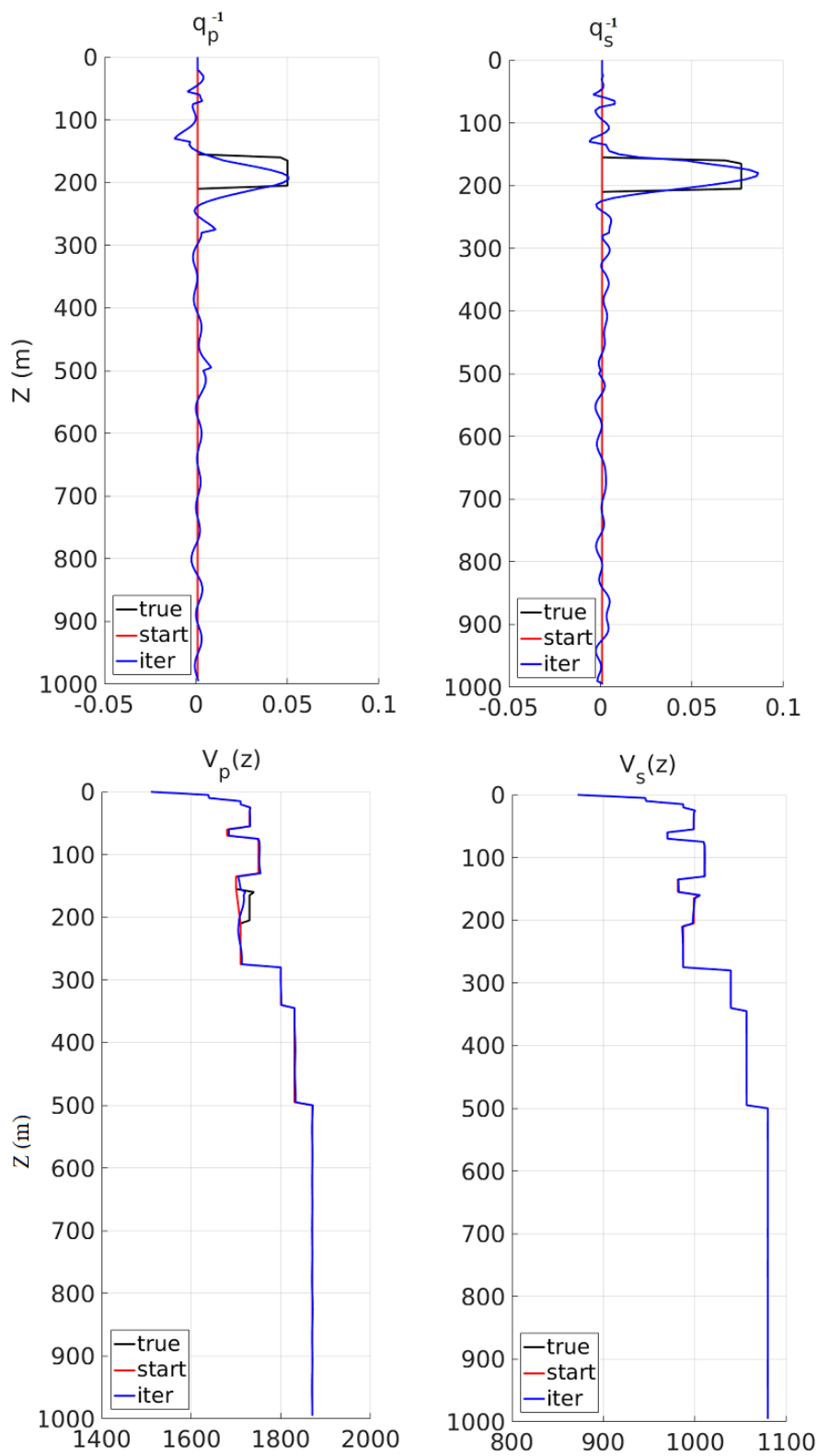


**Figure 7.** Parameters of a viscoelastic medium recovered by multiparameter FWI

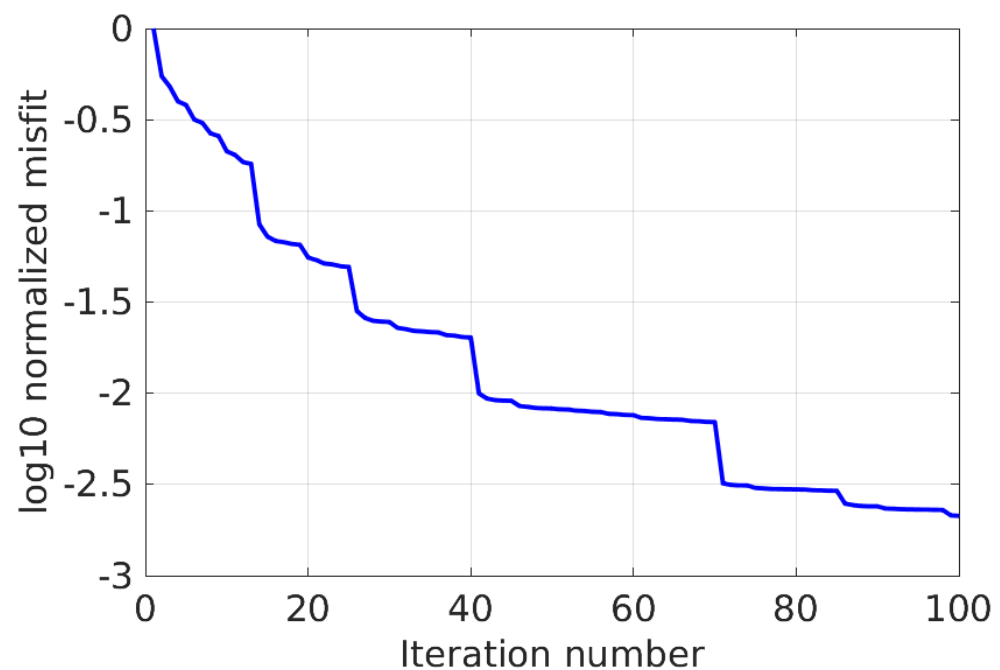


**Figure 8.** Step-wise decrease of the objective functional

makes it possible to restore with sufficient accuracy all the parameters of a viscoelastic medium - the velocity and quality factor of P- and S-waves. At the same time, it should be emphasized that the stability of the solution of the multiparameter inverse seismic problem considered in this paper for a viscoelastic medium is achieved due to the availability of a priori information about the location of methane hydrate accumulations. To describe their localization, we performed predictive modeling focused on recovery of the location of the methane hydrate stability zone.

Thus, carrying out a two-stage hybrid study allows not only localizing the stability zones of methane hydrates with acceptable accuracy, but also assessing their state in order to predict possible emergency situations associated with their decomposition with methane release.

## 6. Conclusions

Violation of the conditions for the formation of the methane hydrate stability zone over the past six thousand years, and, consequently, the possible degradation of gas hydrates at a depth of 100-165 m below the bottom, has led to the accumulation of methane in frozen and cooled horizons of bottom sediments. Subsequent permafrost thaw that is currently taking place and is likely to continue in the near future, may cause an increase in the permeability of bottom rocks, followed by an increase in the emission of methane into the atmosphere from some areas of the shallow water shelf. Therefore, monitoring the process of increasing bottom temperature, which causes thawing of permafrost, accompanied by thawing and degradation of gas hydrates with massive release of methane is an extremely important and urgent task in the light of the changing climate of the Arctic caused by global warming, as well as the expanding activity of geological exploration and the construction of various complex engineering structures associated with this, such as production and injection wells, drilling platforms and pipeline systems.

**Author Contributions:** V.Cheverda and D.Bratchikov are responsible for numerical implementation of FWI algorithm for viscoelastic media and corresponding software development, supported by the project 22-11-00104 of the Russian Science Foundation

E.Golubeva, V.Malakhova and G.Reshetova perform numerical experiments to analyze formation of sub sea permafrost and peculiarities of the seismic waves' propagation in viscoelastic media,

supported by the project 20-11-201112 of the Russian Science Foundation  
K.Gadylshin implement analysis of the coupling of parameters for viscoelastic inversion, supported by the project 22-21-00738 of the Russian Science Foundation

**Funding:** This research was funded by the following three projects of the Russian Science Foundation: 22-11-00104, 20-11-20112 and 22-21-00738.

**Data Availability Statement:** Any data are delivered by the request to Vladimir Cheverda via e-mail [vova\\_chev@mail.ru](mailto:vova_chev@mail.ru)

**Conflicts of Interest:** The authors declare no conflict of interest.

## Abbreviations

The following abbreviations are used in this manuscript:

DOAJ	Directory of open access journals
FWI	Full Waveform Inversion
MHSZ	Methane hydrate stability zone
MDPI	Multidisciplinary Digital Publishing Institute
PERMB	The lower boundary of permafrost
PERMT	The upper boundary of permafrost

1. Blanch, J.O.; Robertsson, J.O.A. and Symes, W.W. Modeling of a constant Q: Methodology and algorithm for an efficient and optimally inexpensive viscoelastic technique. *Geophysics* **1995**, *60*(1), 176–184.
2. V. Bogoyavlensky. Prospects and problems of the Arctic shelf oil and gas field development // *Burenie i nef't*. 11, 2012. p. 4–10 (in Russian)
3. Chuvilin, E.M.; Bukhanov, B.A.; Tumskey, V.E.; Shakhova, N.E.; Dudarev, O.V.; Semiletov, I.P. Thermal conductivity of bottom sediments in the region of Buor-Khaya Bay (shelf of the Laptev Sea). *Earth's Cryosph.* 2013, *17*, 32–40.
4. Collett, T. S., Lee, M. W., Agena, W. F., Miller, J. J., Lewis, K. A., Zyrianova, M. V., et al. *Permafrost-associated natural gas hydrate occurrences on the Alaska North Slope*, Marine and Petroleum Geology **28**(2) (2011), 279–294. <https://doi.org/10.1016/j.marpetgeo.2009.12.001>
5. Dmitrenko, I., Kirillov, S., Tremblay, L., Kassens, H., Anisimov, O., Lavrov, S., Razumov, S., Grigoriev, M.: Recent changes in shelf hydrography in the Siberian Arctic: Potential for subsea permafrost instability. *J. Geophys. Res.* Vol. 116: C10027. (2011)
6. A.Fichtner. Full Seismic Waveform Modeling and Inversion. Springer, 2011.
7. Gavril'ev, R.G. Catalog of Thermophysical Properties of Rocks in the North-East of Russia; Melnikov Institute of Permafrost SB RAS: Yakutsk, Russian, 2013; 172 p. ISBN 978-5-93254-124-1 300. (In Russian)
8. Gavrilov, A., Malakhova, V., Pizhankova, E. The role of paleogeographic events in the evolution and current state of the East Siberian Shelf permafrost // *Proc. SPIE*. 2021. 11916, 1191656; <https://doi.org/10.1117/12.2602055>
9. Gavrilov A., V.Malakhova, E.Pizhankova, A.Popova *Permafrost and gas hydrate stability zone of the glacial part of the East Siberian shelf*, *Geosciences*, **10**, 2020, 484. <https://doi.org/10.3390/geosciences10120484>
10. Guo, H., X.Wang, J.Jiao, H.Chen *Rock Physics Model and Seismic Dispersion and Attenuation in Gas Hydrate-Bearing Sediments*, *Frontiers in Earth Science*, **18 March 2021**.
11. Q.Hao, S.Greenhalgh. The generalized standard-linear-solid model and the corresponding viscoacoustic wave equations revisited. *Geophysical Journal International* 2019, *219*, 1939 - 1947.
12. Hölemann, J.A, Kirillov, S., Klagge, T., Novikhin, A., Kassens, H. and Timokhov, L.: Near-bottom water warming in the Laptev sea in response to atmospheric and sea-ice conditions in 2007. *Polar Research*. Vol.30: 6425. (2011)
13. James, R., Bousquet, P., Bussmann, I., Haeckel, M., Kipfer, R., Leifer, I., Niemann, H., Ostrovsky, I., Piskozub, J., Rehder, G., Treude, T., Vielstädte, L., and Greinert, J.: Effects of climate change on methane emissions from seafloor sediments in the Arctic Ocean: A review, *Limnol. Oceanogr.*, *61*, S283–S299, <https://doi.org/10.1002/lno.10307>, 2016.

14. Janout, M., J. Hölemann, B. Juhls, T. Krumpfen, B. Rabe, D. Bauch, C. Wegner, H. Kassens, and L. Timokhov. Episodic warming of near-bottom waters under the Arctic sea ice on the central Laptev Sea shelf. *Geophys. Res. Lett.*, Vol.43(1):264–272. (2016)
15. Knyazev, A. V., Lashuk, I. *Steepest Descent and Conjugate Gradient Methods with Variable Preconditioning*. SIAM Journal on Matrix Analysis and Applications. **29** (4) 1267, 2008.
16. Kvenvolden K.A., 1994. Natural Gas Hydrate Occurrence and Issues. *Annals of the New York Academy of Sciences* 715, 236–242
17. Liu, H.-P., Anderson, D.L., Kanamori, H. Velocity dispersion due to anelasticity; implications for seismology and mantle composition. *Geophysics* **1976**, 47, 41–58.
18. Malakhova, V.: The response of the Arctic Ocean gas hydrate associated with subsea permafrost to natural and anthropogenic climate changes, IOP Conf. Ser.: Earth and Environ.l Sci., 606, 012 035, <https://doi.org/10.1088/1755-1315/606/1/012035>, 2020.
19. Malakhova, V. and Eliseev, A.: Salt diffusion effect on the submarine permafrost state and distribution as well as on the stability zone of methane hydrates on the Laptev Sea shelf, *Ice and Snow*, 60, 533–546, <https://doi.org/10.31857/S2076673420040058>, [in Russian], 2020
20. Malakhova, V., Golubeva, E. Model Study of the Effects of Climate Change on the Methane Emissions on the Arctic Shelves // *Atmosphere* 13, 274 (2022). <https://doi.org/10.3390/atmos13020274>
21. McGuire, A., Anderson, L., Christensen, T., Dallimore, S., Guo, L., Hayes, D., Heimann, M., Lorenson, T., Macdonald, R., and Roulet, N.: Sensitivity of the carbon cycle in the Arctic to climate change, *Ecol. Monographs*, 79, 523–555, <https://doi.org/10.1890/08-2025.1>, 2009.
22. Nocedal J., Wright S. J. *Numerical Optimization*, Springer N.Y., 2006, 562 p.
23. Parra, J.O., Hackert, C. Wave attenuation attributes as flow unit indicators. *The Leading Edge* **2002**, 21(6), 564–572.
24. E.Polag, G.Ribiere *Note sur la convergence de méthodes de directions conjuguées* R.I.R.O., **3:16**, 35 - 43, 1969.
25. Portnov, A., Smith, A. J., Mienert, J., Cherkashov, G., Rekant, P., Semenov, P., et al. *Offshore permafrost decay and massive seabed methane escape in water depths 20m at the South Kara Sea shelf*, *Geophysical Research Letters* **40** (2013), 3962–3967. <https://doi.org/10.1002/grl.50735>
26. Rekant, P., Bauch, H. A., Schwenk, T., Portnov, A., Gusev, E., Spiess, V., et al. *Evolution of subsea permafrost landscapes in Arctic Siberia since the Late Pleistocene: A synoptic insight from acoustic data of the Laptev Sea*, *Arktos*, **1(1)**, (2015), 11. <https://doi.org/10.1007/s41063-015-0011-y>
27. Romanovskii, N.N.; Hubberten, H.-W.; Gavrilov, A.V.; Eliseeva, A.A.; Tipenko, G.S. Offshore permafrost and gas hydrate stability zone on the shelf of East Siberian Seas. *Geo-Mar. Lett.* 2005, 25, 167–182.
28. Ruppel, C. D. *Permafrost-associated gas hydrate: Is it really approximately 1% of the global system?*, *Journal of Chemical & Engineering Data*, **60(2)**, (2015) 429–436. <https://doi.org/10.1021/je500770m>
29. Ruppel, C. D., & Waite, W. F. *Timescales and processes of methane hydrate formation and breakdown, with application to geologic systems* *Journal of Geophysical Research: Solid Earth*, 125, e2018JB016459. <https://doi.org/10.1029/2018JB016459>
30. Reagan, M. and Moridis, G. *Dynamic response of oceanic hydrate deposits to ocean temperature change* *J. Geophys. Res.: Oceans*, 113, C12 023, <https://doi.org/10.1029/2008JC004938>, 2008.
31. Sun, Y.F., Goldberg, D. Hydrocarbon signatures from high-resolution attenuation profiles, SEG Technical Program Expanded Abstracts, 1998, 996–999.
32. Shakhova, N., Semiletov, I., and Chuvilin, E.: Understanding the permafrost-hydrate system and associated methane releases in the East Siberian Arctic Shelf, *Geosciences*, 9, 251, <https://doi.org/10.3390/geosciences9060251>, 2019.
33. Vishnevsky, D., V.Lisitsa, G.Reshetova *Numerical simulation of seismic wave propagation in media with viscoelastic intrusions* *Numerical methods and programming*, **14: 1**, 155 - 165, 2013
34. Wilkenskeld S. , Miesner F., Overduin P.P., Puglini M., Brovkin V. Strong increase in thawing of subsea permafrost in the 22nd century caused by anthropogenic climate change // *The Cryosphere* 16 (3), 1057–1069, 2022.
35. Yurganov L.N., Leifer I. Estimates of methane emission rates from some Arctic and sub-Arctic areas based on orbital interferometer IASI data // *Sovremennye problemy dstantsionnogo zondirovaniya Zemli iz kosmosa*. 2016. V. 13. No. 3. P. 173–183 (in Russian) [Author1(year)]ref-journal Author 1, T. The title of the cited article. *Journal Abbreviation* **2008**, 10, 142–149.
36. Author 2, L. The title of the cited contribution. In *The Book Title*; Editor 1, F., Editor 2, A., Eds.; Publishing House: City, Country, 2007; pp. 32–58.
37. Author 1, A.; Author 2, B. *Book Title*, 3rd ed.; Publisher: Publisher Location, Country, 2008; pp. 154–196.

- 
38. Author 1, A.B.; Author 2, C. Title of Unpublished Work. *Abbreviated Journal Name* year, *phrase indicating stage of publication (submitted; accepted; in press)*.
  39. Author 1, A.B. (University, City, State, Country); Author 2, C. (Institute, City, State, Country). Personal communication, 2012.
  40. Author 1, A.B.; Author 2, C.D.; Author 3, E.F. Title of presentation. In Proceedings of the Name of the Conference, Location of Conference, Country, Date of Conference (Day Month Year); Abstract Number (optional), Pagination (optional).
  41. Author 1, A.B. Title of Thesis. Level of Thesis, Degree-Granting University, Location of University, Date of Completion.
  42. Title of Site. Available online: URL (accessed on Day Month Year).